

Photon-Pair Production and Frequency Translation using Backward-Wave Spontaneous Parametric Downconversion

PAULINA S. KUO,^{1,*} DILEEP V. REDDY,^{2,3} VARUN VERMA,³ SAE WOO NAM,³ ANDRIUS ZUKAUSKAS,⁴ AND CARLOTA CANALIAS⁴

¹*Information Technology Laboratory, National Institute of Standards and Technology, 100 Bureau Drive, Gaithersburg, MD 20899*

²*Department of Physics, University of Colorado Boulder, Boulder, CO 80309*

³*Physical Measurement Laboratory, National Institute of Standards and Technology, 325 Broadway, Boulder, CO 80305*

⁴*Department of Applied Physics, KTH—Royal Institute of Technology, AlbaNova Universitetscentrum, 10691 Stockholm, Sweden*

*paulina.kuo@nist.gov

Abstract: Backward-wave three-wave mixing is a difficult $\chi^{(2)}$ interaction to observe because it requires ultrashort poling periods to achieve phasematching. Having realized sub-micrometer periods in periodically poled KTiOPO₄ (PPKTP), we demonstrate for the first time first-order quasi-phasematched, backward-wave spontaneous parametric downconversion (BW SPDC). We pumped the PPKTP crystal at 800 nm and obtained a forward-wave signal at 1400 nm and a backward-wave idler at 1868 nm. We estimated an internal pair production rate of 4.0×10^4 pairs/s/mW. The backward-wave phasematching constraints lead to the unique tuning property that spectral features of the pump are transferred to the forward-wave signal photons, which makes BW SPDC an attractive source of spectrally shaped, heralded single photons. These spectrally shaped photons are useful for quantum computing and quantum interconnects. For the first time, we experimentally show this effect by observing frequency translation between a spectrally shaped pump beam and the BW SPDC signal photons. Due to their unique properties, BW-SPDC-based devices will be important building blocks for quantum information processing.

1. Introduction

Backward-wave (BW) three-wave mixing was first proposed by S. E. Harris in 1966 [1]. However, due to the very small quasi-phasematching (QPM) [2, 3] periods required (typically less than 1 μm for first-order QPM), it was not experimentally realized until 2007 in a backward-wave optical parametric oscillator (BW OPO) [4]. Since then, substantial progress in fabrication of QPM gratings with sub-micrometer periodicities has been made, allowing further experimental studies of BW OPOs [5–9]. For backward-wave spontaneous parametric downconversion (BW SPDC), there have been several theoretical studies [10–16] highlighting the unique features of BW SPDC, which include having highly narrowband idler [10, 13] and separable joint spectral amplitude [11, 15]. However, the only few experimental studies have utilized third-order [17] and fifth-order [18–20] QPM gratings, which have low conversion efficiencies. Thanks to the progress in ultrashort-period, periodically poled Rb-doped KTiOPO₄ (PPKTP) [9, 21, 22], we can now report on the first demonstration of BW SPDC in a first-order, PPKTP grating having 500 nm period and direct measurement of the SPDC spectra. We further show that BW SPDC can be used to generate spectrally shaped, heralded single photons, which are useful for quantum networking [23, 24], quantum interconnects [25] and quantum information processing [26].

One key application of BW SPDC is in producing spectrally shaped, single photons. These are useful for optical quantum computing where the qubits are encoded in frequency bins [26]. Also, spectrally shaped single photons will be needed in the quantum interconnects between different quantum nodes in a quantum network. These nodes may be based on different technologies

such as atomic ensembles [23, 27], trapped ions [28], or nitrogen-vacancy centers [29]. The operating wavelengths, linewidths and other spectral requirements of these nodes may be different, which will require quantum frequency conversion [30], filtering [31] or spectral engineering of entangled photons [32] to connect the nodes. BW SPDC represents a new way to generate spectrally tailored photons.

Spectral shaping of single photons using BW SPDC has advantages over existing techniques. SPDC photons are typically shaped after they are generated using programmable filters or spatial light modulators [32, 33]. These techniques cause some loss of the downconverted photons, break apart photon pairs and reduce the SPDC pair generation efficiency. In contrast for BW SPDC, spectral shaping is applied to the pump and then transferred to the downconverted single photons through the process of frequency translation [7, 34]. Losses due to spectral shaping of the pump beam can be compensated by increasing the pump power without degrading the SPDC pair generation efficiency. The improvement in generation efficiency and avoidance of losses are very attractive features for quantum networking and quantum computing. Another method for spectrally shaping SPDC photons is to engineer the nonlinear optical medium by incorporating an optical cavity [35] or by aperiodic-domain-engineering of the nonlinear crystal [36–38], but the spectral shape is fixed during fabrication and does not offer reconfigurability.

In BW three-wave mixing, the pump and signal are co-propagating while the idler is counter-propagating. The phase-mismatch, Δk , is given by

$$\Delta k = k_p - k_s + k_i = 2\pi \left(\frac{n_p}{\lambda_p} - \frac{n_s}{\lambda_s} + \frac{n_i}{\lambda_i} \right) = \frac{2\pi m}{\Lambda_G}, \quad (1)$$

where $k_j = 2\pi n_j / \lambda_j$, n_j is the refractive index, λ_j is the wavelength of wave j ; and p, s and i refer to the pump, signal and idler respectively. The required QPM period, Λ_G , is $2\pi m / \Delta k$ where m is the QPM order [3]. The sign of k_i is reversed compared to the conventional co-propagating idler case, which results in large Δk requiring small Λ_G / m . First order ($m = 1$) QPM is desirable because it gives the largest nonlinear conversion efficiency, but it is very challenging due to the sub-micron QPM periods needed. Typically, the BW idler has the longest wavelength of the three interacting waves. However, it is possible for the counter-propagating wave to have the intermediate wavelength.

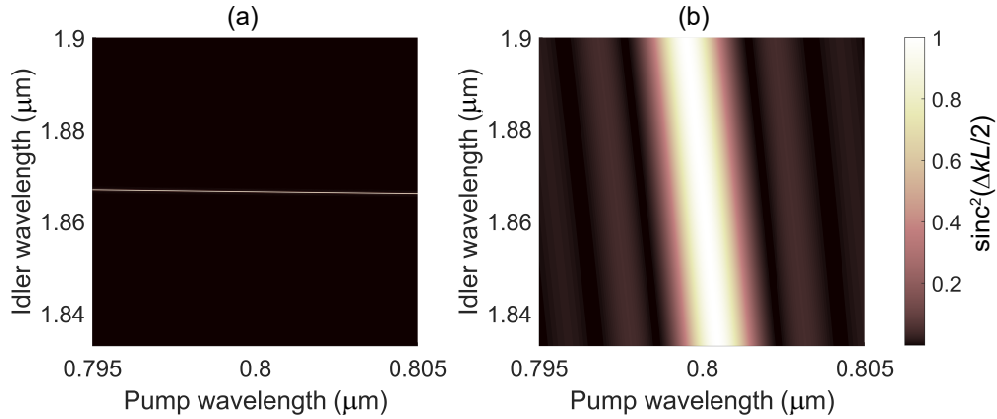


Fig. 1. Using the same pump, signal and idler that are all z -polarized, theoretical idler tuning for (a) BW and (b) forward-wave (FW) downconversion as the pump is varied near 800 nm in a 6 mm long PPKTP crystal. The BW case shows highly narrowband idler that is nearly insensitive to pump tuning. The poling periods are 0.5 μm for the BW case and 26.3 μm for the FW case.

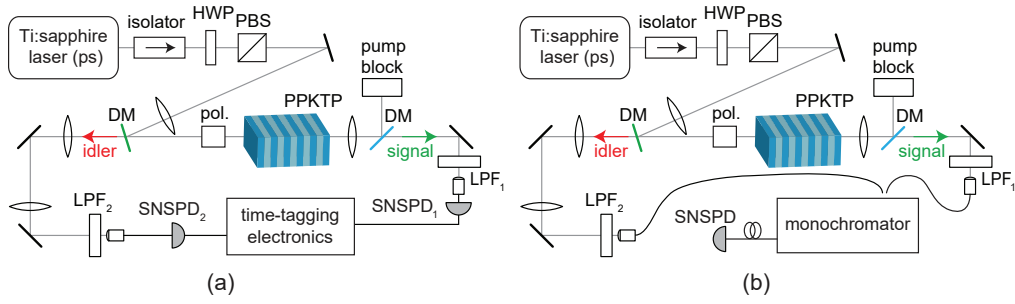


Fig. 2. Experimental setups for measuring (a) coincidences and (b) spectra using a fiber-coupled monochromator. The 1.6-ps duration Ti:sapphire laser pumps the PPKTP crystal. The signal and idler are collected into fibers and sent to SNSPD₁ and SNSPD₂, respectively. The collection fibers are alternately connected to the monochromator to record the spectra. HWP, half-wave plate; PBS, polarizing beam splitter; DM, dichroic mirror; pol., polarizer; LPF, long-pass filter.

The unique tuning behaviors of BW three-wave-mixing devices arising from their k -vector constraints have been previously noted [4, 6–8, 10, 14, 34, 39]. These unique tuning behaviors include having highly narrowband backward-propagating idler wave and weak dependence of the idler frequency with respect to the pump frequency ($\partial\omega_i/\partial\omega_p \approx -0.01$ [7], where ω_j refers to the angular frequency of wave j), which is illustrated in Fig. 1. Another tuning behavior of BW three-wave mixing is that the forward-propagating signal wave has a frequency response that mimics that of the pump wave. This observation led to the proposal that BW devices can be used as frequency translators between the pump and signal wavelengths [7, 34]. This frequency-translation property follows from having highly narrowband idler that is insensitive to pump tuning; by energy conservation, the spectral information of the pump wave is translated onto the forward-propagating signal wave. In this work, we experimentally investigate frequency translation using BW SPDC.

2. Experimental Setup

We demonstrated BW SPDC using a first-order PPKTP crystal having 500 nm QPM period. The fabrication of this PPKTP crystal was performed via coercive field engineering and is described in [9, 22]. The crystal was designed to have all waves z -polarized (type-0) with wavelengths $800 \text{ nm} \rightarrow 1.4 \mu\text{m} + 1.87 \mu\text{m}$, and it was uncoated and operated at room temperature. The PPKTP grating was 6 mm long, 3 mm wide and 1 mm thick. Figure 2 sketches the experimental setups. The pump was a mode-locked Ti:sapphire laser with transform-limited 1.6 ps pulse duration, and 76 MHz repetition rate focused to $44 \mu\text{m}$ beam waist. A Glan-Taylor polarizer was placed before the PPKTP crystal to ensure the pump was polarized along the crystal z -direction. Dichroic mirrors (DM) that reflect the pump and transmit the signal and idler were used to direct the pump to the crystal and reject it afterwards. The forward-going signal and backward-going idler were coupled into SMF28 fibers and sent to superconducting nanowire single-photon detectors (SNSPD₁ and SNSPD₂ for the signal and idler, respectively). Long-pass filters (LPFs) were placed before the fiber couplers to remove any residual pump photons.

To detect the infrared photons, we used SNSPDs with broadband infrared sensitivity coupled to SMF28 single-mode fibers. The fibers connected to SNSPD₁ (signal) and SNSPD₂ (idler) were coiled with 40 mm and 60 mm diameters, respectively, to reduce dark counts caused by blackbody radiation while transmitting the wavelengths of interest [40]. The tighter coils for SNSPD₁ resulted in lower dark count rates but excess attenuation at the $1.87 \mu\text{m}$ idler. We estimated the system detection efficiency of SNSPD₁ to be 88% at 1400 nm, and SNSPD₂ to be

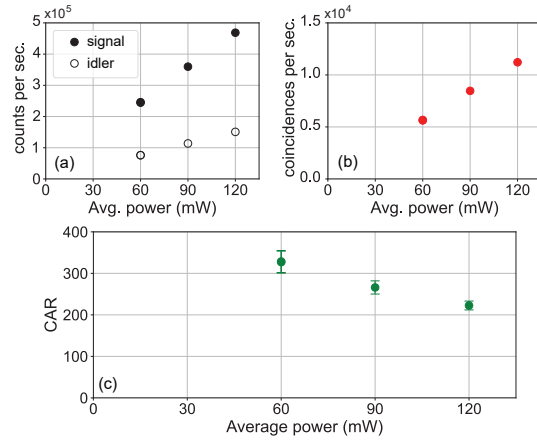


Fig. 3. Measured (a) single-channel and (b) coincidences count rates. (c) CAR as a function of incident average pump power.

85% at 1875 nm. Using these SNSPDs, we detected SPDC from the PPKTP and also analyzed the spectra of the downconverted photons by passing them through a grating monochromator (Fig. 2b).

To observe the frequency translation of spectral properties from the pump to the signal, we used self-phase modulation (SPM) [41] to create a spectrally modulated pump. A 3.2-meter-long section of HI780 fiber was inserted in the experimental setup between the PBS and focusing lens before the PPKTP crystal. The coupling efficiency into the HI780 fiber was about 56%. The polarization from the fiber was adjusted using a fiber polarization controller to maximize the transmission through the polarizer placed before the PPKTP crystal. We measured the power before the polarizer, and after the PPKTP crystal (the latter, at the pump block in Fig. 2). We held the ratio of these powers constant (at $70\% \pm 1\%$) while changing the Ti:sapphire laser power using the half-waveplate (HWP in Fig. 2), thereby changing the amount of self-phase modulation on the pump.

3. Results

Figure 3 shows the measured signal and idler count rates, and coincidence rates for BW SPDC. Using 60 mW incident average power from the mode-locked Ti:sapphire laser, we observed 2.5×10^5 counts/s at the signal and 7.6×10^4 counts/s at the idler (with background count rates of 1.7×10^3 counts/s and 3.8×10^3 counts/s at the respective detectors). The coincidence rate was 5.7×10^3 coincidences/s and the coincidences-to-accidentals ratio (CAR) was 330 ± 26 (where the uncertainty is calculated by assuming Poisson statistics for the observed counts). We estimated the signal and idler collection efficiencies [42] to be 8.5% and 2.7%, respectively, which include detector efficiencies and losses in the paths between the crystal and the detectors (i.e., losses from the uncoated crystal, optical elements, fiber coupler, etc.). From these data, we calculated the internal pair production rate to be 4.0×10^4 pairs/s/mW. As a comparison, BW SPDC in a type-0, fifth-order QPM, periodically poled LiNbO₃ (PPLN) waveguide exhibited internal pair production rate of 5 pairs/s/mW [20] using similar pulsed pumping. Table 1 presents a comparison of our result with other BW SPDC experiments. The internal pair generation rate is expressed in terms of the average pump power, so we also include the pump duration (τ_{pump}) and pump repetition rate in the table for clarity.

We performed a direct measurement of the SPDC spectra by sending the fiber-coupled SPDC photons to a grating monochromator (with 1/3 m focal length and 600 groove/mm grating blazed

Table 1. Comparison of Several BW SPDC Experiments

Description	Period (μm)	QPM order	Length (mm)	τ_{pump} (ps)	Pump rep. rate (MHz)	Internal gen. rate (pairs/s/mW) ¹
PPKTP bulk, type-0 (this work)	0.5	1	6	1.6	76	4.0×10^4
PPKTP waveguide, type-2 [17]	1.3	3	10	2	— ^b	2.1×10^4
PPLN waveguide, type-0 [20]	1.7	5	37	2	80	5×10^0
PPKTP waveguide, type-0 [19]	2.0	5	7	100	18	— ^c

^aGeneration rate is given per average pump power.

^bRef. [17] does not report pump repetition rate.

^cRef. [19] lists the internal generation rate as 63 kHz-mW.

at 1.5 μm) connected to SNSPD₂. The incident average pump power was 120 mW. Figure 4a shows the pump transmitted through the PPKTP crystal, while Figs. 4b and 4c show the signal and idler spectra. The signal was detected at 1400 nm and the idler at 1868 nm, which agreed well with phasematching predictions [43]. We note that the spectral scans were limited by the step size rather than by the instrument resolution. The reciprocal linear dispersion (RLD) of the monochromator was 1.16 nm/mm, and the monochromator slit size was 2 mm. However, the exit-aperture size of the monochromator was set by the collection fiber (with aperture width on the order of 10 μm). The monochromator resolution is the RLD multiplied by the aperture size or approximately 0.02 nm. In comparison, the minimum step size was about 0.5 nm, which is larger than the theoretically predicted BW idler bandwidth of 12 GHz (or 0.14 nm).

We also investigated wavelength tuning of BW SPDC. Figure 5 shows the effect of tuning the pump wavelength by 5 nm (from 800 nm to 805 nm) while keeping other parameters the same (temperature, pump power, etc.). Spectra represented by solid lines in Figure 5 have 800 nm pump wavelength while the dashed lines have 805 nm pump wavelength. We see that the idler wavelength is nearly unchanged; $\Delta\lambda_i = -0.5$ nm, which is the step size for the monochromator scan. The change in the signal (measured in wavenumber, $\tilde{\nu}$, where $\tilde{\nu} = 1/\lambda$) is $\Delta\tilde{\nu}_s = -76$ cm^{-1} , which is nearly equal to the change in the pump, $\Delta\tilde{\nu}_p = -78$ cm^{-1} . This tuning behavior matches

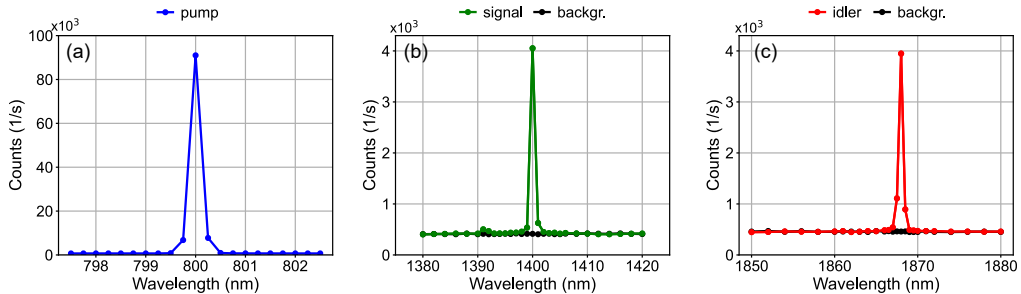


Fig. 4. Measured spectra for the (a) pump transmitted through the PPKTP, (b) signal and (c) idler. For the latter, we also show the background counts (measured with the pump to the experiment blocked).

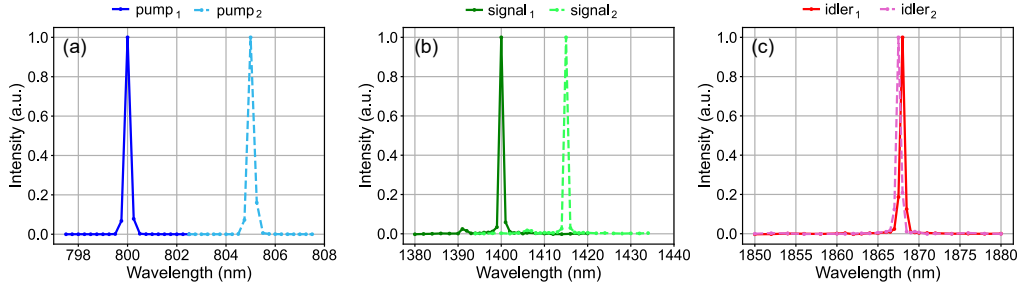


Fig. 5. Normalized and background-subtracted BW SPDC spectra for 800-nm and 805-nm pumping. The solid curves represent results from 800 nm pump while the dashed curves have 805 nm pump. (a) Pump transmitted through the PPKTP, and generated (b) signal and (c) idler. The backward-wave idler shows very weak tuning as a function of pump tuning.

the behavior seen previously in BW OPOs [4], where the backward-wave frequency depends very weakly on the pump frequency.

We investigated frequency translation of spectral properties from the BW SPDC pump to the signal photons. We passed the pump through a length of fiber that produced self-phase modulation to create different modulated pump spectra. Figure 6a shows the pump spectra measured with the monochromator at several different pump powers. The listed average powers represent the pump power after the SPM fiber and before the PPKTP and polarizer. We see the pump spectrum becomes increasingly distorted at higher pump powers. In Fig. 6b, we plot the measured idler spectra. We observed that the idler remains narrowband and centered at 1867.5 nm. Figures 6c-6e show the measured signal spectra and the translated pump spectra at the three power levels. The translated pump wavelengths were calculated by assuming the idler to be highly narrowband and fixed at $\lambda_{i,0} = 1867.5$ nm, and applying energy conservation such that $1/\lambda_{\text{trans}} = 1/\lambda_p - 1/\lambda_{i,0}$. There is good agreement between the signal spectra and the translated pump spectra. By using the idler as the heralding photon, the signal photon can be used as a spectrally shaped, heralded single photon.

4. Discussion

BW SPDC is a novel, unique source of photon pairs that will be useful for quantum information processing. With advances in ultra-short-period PPKTP crystals [9,22,44], higher pair-generation efficiencies through first-order phasematching can be achieved. As even shorter periods become available, shorter visible-wavelength photon pairs can be produced. BW SPDC is attractive since the output photons naturally emerge from two different ports. The BW SPDC two-photon state will have minimal spectral correlations and a nearly separable joint spectra amplitude [11, 15–17, 20], which is useful so that spectral filtering of the SPDC output can be avoided and higher count rates can be achieved [45].

The frequency-translation properties of BW SPDC will enable design of efficient, spectrally shaped, heralded single-photon sources. Frequency translation allows the spectral shaping to occur on the pump beam before the photon pairs are generated. This is in contrast to conventional SPDC spectral-shaping where losses due to the shaping are imposed on the downconverted photons, which reduces the pair generation efficiency.

It has been noted that frequency and phase translation using spontaneous BW three-wave mixing differs from that of optical parametric amplification (OPA) [6]. OPA acts as a perfect phase-sensitive amplifier [46], which enables processes like quantum frequency conversion (QFC) [30] or quantum frequency translation (QFT) [47], where the quantum state can be

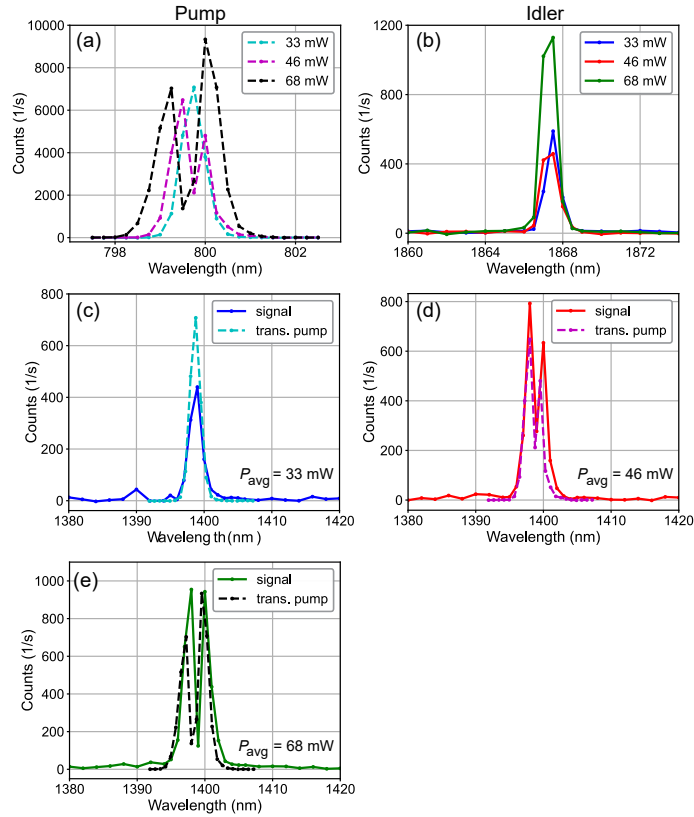


Fig. 6. Spectra of BW SPDC using a self-phase modulated pump. (a) Pump spectra with SPM and (b) BW SPDC idler spectra at different average pump powers, P_{avg} . Comparisons of SPDC signal spectra with translated pump spectra for P_{avg} of (c) 33 mW, (d) 46 mW and (e) 68 mW. The counts for the translated pump spectra are reduced by a factor of 10 for easy comparison.

transferred from light at one frequency to another frequency. In spontaneous BW three-wave mixing, the momentum conservation condition (Eq. 1) forces the counter-propagating idler to be nearly stationary in frequency, which gives rise to frequency translation from the pump to the signal. However, this transfer is only approximate and not perfect since the idler is not perfectly stationary and the phase of the counter-propagating idler is only approximately constant [6]. It follows that spectral shaping can be transferred between the pump and signal using BW SPDC, but BW SPDC can not be used for transfer of the quantum state. We also note that in QFC and QFT, the stationary beam is the high-power pump, while in BW SPDC frequency translation, the stationary beam is the low-power idler.

Frequency translation using BW SPDC has similarities to group-velocity-engineered SPDC [48]. When the group velocity of the pump matches that of the signal (using asymmetric group-velocity-matching (aGVM)), the spectral shape of the signal can be programmed by the spectral shape of the pump. However, bandwidth of the idler in aGVM SPDC is not nearly as narrow as in BW SPDC, so the spectrum of the signal will not track as closely to the pump compared to BW SPDC.

In the future, we plan to improve the spectral measurements of BW SPDC by exploring other techniques, including time-of-flight spectroscopy [49], stimulated emission tomography [50] and use of scanning Fabry-Perot interferometers (FPIs) [51, 52]. One of the challenges with first-order BW three-wave mixing is that the idler tends to have long wavelength (typically longer than 1550

nm). At these long wavelengths, fiber-based dispersion modules are not available, which makes time-of-flight spectroscopy [49] difficult to perform. Using stimulated emission tomography [50], it would be possible to seed the BW SPDC at 1400 nm and observe the output through difference frequency generation. This technique can provide detailed spectral information about the BW SPDC process, but it is not a direct observation of the SPDC. The use of scanning FPIs is also a promising technique for probing single-photon-level spectra [52], but short cavity lengths (5 mm or shorter) are needed to have sufficiently wide free-spectral range to observe the predicted 12 GHz bandwidth idler.

5. Conclusion

For the first time, we experimentally observed backward-wave SPDC in a first-order quasi-phases-matched crystal. The 500 nm period PPKTP crystal produced forward-wave signal at 1400 nm and backward-wave idler at 1868 nm when pumped at 800 nm. We observed 1.1×10^4 coincidences/s using 60 mW average pump power. Using estimated signal and idler collection efficiencies, we inferred the internal pair production rate to be 4.0×10^4 pairs/s/mW. The output spectra of the BW SPDC were directly measured with a grating monochromator. We verified the phasematching wavelengths and confirmed that the backward-wave idler was nearly stationary in frequency and narrow in bandwidth. We also demonstrated for the first time frequency translation using BW SPDC where the spectral properties of the pump wave are transferred to the signal wave. BW SPDC can be used as a source of spectrally shaped, heralded single photons that can be used in quantum networks, quantum interconnects and photonic quantum computing.

Disclosures. The authors declare no conflicts of interest. Certain commercial equipment or materials may be identified in this paper in order to specify device fabrication, the experimental procedure and data analysis adequately. Such identification is not intended to imply endorsement by the National Institute of Standards and Technology, nor is it intended to imply that the equipment or material identified are necessarily the best available.

Data Availability Statement. Data underlying the results presented in this paper are available in Ref. [53].

References

1. S. E. Harris, "Proposed backward wave oscillation in the infrared," *Appl. Phys. Lett.* **9**, 114–116 (1966).
2. J. A. Armstrong, N. Bloembergen, J. Ducuing, and P. S. Pershan, "Interactions between light waves in a nonlinear dielectric," *Phys. Rev.* **127**, 1918–1939 (1962).
3. M. Fejer, G. Magel, D. Jundt, and R. Byer, "Quasi-phase-matched second harmonic generation: tuning and tolerances," *IEEE J. Quantum Electron.* **28**, 2631–2654 (1992).
4. C. Canalias and V. Pasiskevicius, "Mirrorless optical parametric oscillator," *Nat. Photonics* **1**, 459–462 (2007).
5. G. Strömqvist, V. Pasiskevicius, and C. Canalias, "Self-established noncollinear oscillation and angular tuning in a quasi-phase-matched mirrorless optical parametric oscillator," *Appl. Phys. Lett.* **98**, 051108 (2011).
6. G. Strömqvist, V. Pasiskevicius, C. Canalias, and C. Montes, "Coherent phase-modulation transfer in counterpropagating parametric down-conversion," *Phys. Rev. A* **84**, 023825 (2011).
7. A.-L. Viotti, F. Laurell, A. Zukauskas, C. Canalias, and V. Pasiskevicius, "Coherent phase transfer and pulse compression at 1.4 μm in a backward-wave OPO," *Opt. Lett.* **44**, 3066–3069 (2019).
8. G. Strömqvist, V. Pasiskevicius, C. Canalias, P. Aschieri, A. Picozzi, and C. Montes, "Temporal coherence in mirrorless optical parametric oscillators," *J. Opt. Soc. Am. B* **29**, 1194–1202 (2012).
9. A. Zukauskas, A.-L. Viotti, C. Liljestränd, V. Pasiskevicius, and C. Canalias, "Cascaded counter-propagating nonlinear interactions in highly-efficient sub- μm periodically poled crystals," *Sci. Reports* **7**, 8037 (2017).
10. M. C. Booth, M. Atatüre, G. Di Giuseppe, B. E. A. Saleh, A. V. Sergienko, and M. C. Teich, "Counterpropagating entangled photons from a waveguide with periodic nonlinearity," *Phys. Rev. A* **66**, 023815 (2002).
11. A. Christ, A. Eckstein, P. J. Mosley, and C. Silberhorn, "Pure single photon generation by type-I PDC with backward-wave amplification," *Opt. Express* **17**, 3441–3446 (2009).
12. T. Suhara and M. Ohno, "Quantum theory analysis of counterpropagating twin photon generation by parametric downconversion," *IEEE J. Quantum Electron.* **46**, 1739–1745 (2010).
13. C.-S. Chuu and S. E. Harris, "Ultrabright backward-wave biphoton source," *Phys. Rev. A* **83**, 061803 (2011).
14. T. Corti, E. Brambilla, and A. Gatti, "Critical behavior of coherence and correlation of counterpropagating twin beams," *Phys. Rev. A* **93**, 023837 (2016).

15. A. Gatti, T. Corti, and E. Brambilla, "Temporal coherence and correlation of counterpropagating twin photons," *Phys. Rev. A* **92**, 053809 (2015).
16. A. Gatti and E. Brambilla, "Heralding pure single photons: A comparison between counterpropagating and copropagating twin photons," *Phys. Rev. A* **97**, 013838 (2018).
17. Y.-C. Liu, D.-J. Guo, K.-Q. Ren, R. Yang, M. Shang, W. Zhou, X. Li, C.-W. Sun, P. Xu, Z. Xie, Y.-X. Gong, and S.-N. Zhu, "Observation of frequency-uncorrelated photon pairs generated by counter-propagating spontaneous parametric down-conversion," *Sci. Reports* **11**, 12628 (2021).
18. A. A. Shukhin, D. O. Akatiev, I. Z. Latypov, A. V. Shkalikov, and A. A. Kalachev, "Simulating single-photon sources based on backward-wave spontaneous parametric down-conversion in a periodically poled KTP waveguide," *J. Physics: Conf. Ser.* **613**, 012015 (2015).
19. I. Latypov, A. Shukhin, D. Akat'ev, A. Shkalikov, and A. Kalachev, "Backward-wave spontaneous parametric down-conversion in a periodically poled KTP waveguide," *Quantum Electron.* **47**, 827 (2017).
20. K.-H. Luo, V. Ansari, M. Massaro, M. Santandrea, C. Eigner, R. Ricken, H. Herrmann, and C. Silberhorn, "Counter-propagating photon pair generation in a nonlinear waveguide," *Opt. Express* **28**, 3215–3225 (2020).
21. C. Canalias, V. Pasiskevicius, R. Clemens, and F. Laurell, "Submicron periodically poled flux-grown KTiOPO₄," *Appl. Phys. Lett.* **82**, 4233–4235 (2003).
22. P. Mutter, A. Zukauskas, and C. Canalias, "Domain dynamics in coercive-field engineered sub- μm periodically poled Rb-doped KTiOPO₄," *Opt. Mater. Express* **12**, 4332–4340 (2022).
23. H. J. Kimble, "The quantum internet," *Nature* **453**, 1023–1030 (2008).
24. S. Pirandola and S. L. Braunstein, "Unite to build a quantum internet," *Nature* **532**, 169–171 (2016).
25. D. Awschalom, K. K. Berggren, H. Bernien, S. Bhave, L. D. Carr, P. Davids, S. E. Economou, D. Englund, A. Faraon, M. Fejer, S. Guha, M. V. Gustafsson, E. Hu, L. Jiang, J. Kim, B. Korzh, P. Kumar, P. G. Kwiat, M. Lončar, M. D. Lukin, D. A. Miller, C. Monroe, S. W. Nam, P. Narang, J. S. Orcutt, M. G. Raymer, A. H. Safavi-Naeini, M. Spiropulu, K. Srinivasan, S. Sun, J. Vučković, E. Waks, R. Walsworth, A. M. Weiner, and Z. Zhang, "Development of quantum interconnects (QICs) for next-generation information technologies," *PRX Quantum* **2**, 017002 (2021).
26. J. M. Lukens and P. Lougovski, "Frequency-encoded photonic qubits for scalable quantum information processing," *Optica* **4**, 8–16 (2017).
27. L.-M. Duan, M. D. Lukin, J. I. Cirac, and P. Zoller, "Long-distance quantum communication with atomic ensembles and linear optics," *Nature* **414**, 413–418 (2001).
28. R. Blatt and D. Wineland, "Entangled states of trapped atomic ions," *Nature* **453** (2008).
29. B. Hensen, H. Bernien, A. E. Dréau, A. Reiserer, N. Kalb, M. S. Blok, J. Ruitenberg, R. F. L. Vermeulen, R. N. Schouten, C. Abellán, W. Amaya, V. Pruneri, M. W. Mitchell, M. Markham, D. J. Twitchen, D. Elkouss, S. Wehner, T. H. Tamminiau, and R. Hanson, "Loophole-free bell inequality violation using electron spins separated by 1.3 kilometres," *Nature* **526**, 682–686 (2015).
30. P. Kumar, "Quantum frequency conversion," *Opt. Lett.* **15**, 1476–1478 (1990).
31. M. Meraner, A. Mazloom, V. Krutyanskiy, V. Krcmarsky, J. Schupp, D. A. Fioretto, P. Sekatski, T. E. Northup, N. Sangouard, and B. P. Lanyon, "Indistinguishable photons from a trapped-ion quantum network node," *Phys. Rev. A* **102**, 052614 (2020).
32. B. Dayan, Y. Bromberg, I. Afek, and Y. Silberberg, "Spectral polarization and spectral phase control of time-energy entangled photons," *Phys. Rev. A* **75**, 043804 (2007).
33. J. M. Lukens, A. Dezfouliyan, C. Langrock, M. M. Fejer, D. E. Leaird, and A. M. Weiner, "Biphoton manipulation with a fiber-based pulse shaper," *Opt. Lett.* **38**, 4652–4655 (2013).
34. A.-L. Viotti, A. Zukauskas, C. Canalias, F. Laurell, and V. Pasiskevicius, "Narrowband, tunable, infrared radiation by parametric amplification of a chirped backward-wave OPO signal," *Opt. Express* **27**, 10602–10610 (2019).
35. M. Kues, C. Reimer, J. M. Lukens, W. J. Munro, A. M. Weiner, D. J. Moss, and R. Morandotti, "Quantum optical microcombs," *Nat. Photonics* **13**, 170–179 (2019).
36. P. S. Kuo, V. B. Verma, and S. W. Nam, "Demonstration of a polarization-entangled photon-pair source based on phase-modulated ppln," *OSA Continuum* **3**, 295–304 (2020).
37. A. Pickston, F. Graffitti, P. Barrow, C. L. Morrison, J. Ho, A. M. Brańczyk, and A. Fedrizzi, "Optimised domain-engineered crystals for pure telecom photon sources," *Opt. Express* **29**, 6991–7002 (2021).
38. C. L. Morrison, F. Graffitti, P. Barrow, A. Pickston, J. Ho, and A. Fedrizzi, "Frequency-bin entanglement from domain-engineered down-conversion," *APL Photonics* **7**, 066102 (2022).
39. A. Godard, M. Guionie, J.-B. Dherbecourt, J.-M. Melkonian, and M. Raybaut, "Backward optical parametric oscillator threshold and linewidth studies," *J. Opt. Soc. Am. B* **39**, 408–420 (2022).
40. P. S. Kuo, "Using silica fiber coupling to extend superconducting nanowire single-photon detectors into the infrared," *OSA Continuum* **1**, 1260–1266 (2018).
41. G. Agrawal, *Nonlinear Fiber Optics* (Academic Press, Oxford, 2013), 5th ed.
42. S. V. Polyakov and A. L. Migdall, "High accuracy verification of a correlated-photon-based method for determining photon-counting detection efficiency," *Opt. Express* **15**, 1390–1407 (2007).
43. K. Fradkin, A. Arie, A. Skliar, and G. Rosenman, "Tunable midinfrared source by difference frequency generation in bulk periodically poled KTiOPO₄," *Appl. Phys. Lett.* **74**, 914–916 (1999).
44. A. Zukauskas, A.-L. Viotti, R. Coetzee, C. Liljestrang, V. Pasiskevicius, and C. Canalias, "Recent advances in sub- μm PPKTP for non-linear interactions with counter-propagating photons," *Proc. SPIE* **10902**, 109020G (2019).

45. W. P. Grice, A. B. U'Ren, and I. A. Walmsley, "Eliminating frequency and space-time correlations in multiphoton states," *Phys. Rev. A* **64**, 063815 (2001).
46. W. H. Louisell, A. Yariv, and A. E. Siegman, "Quantum fluctuations and noise in parametric processes. I." *Phys. Rev.* **124**, 1646–1654 (1961).
47. H. J. McGuinness, M. G. Raymer, and C. J. McKinstrie, "Theory of quantum frequency translation of light in optical fiber: application to interference of two photons of different color," *Opt. Express* **19**, 17876–17907 (2011).
48. V. Ansari, J. M. Donohue, B. Brecht, and C. Silberhorn, "Tailoring nonlinear processes for quantum optics with pulsed temporal-mode encodings," *Optica* **5**, 534–550 (2018).
49. M. Avenhaus, A. Eckstein, P. J. Mosley, and C. Silberhorn, "Fiber-assisted single-photon spectrograph," *Opt. Lett.* **34**, 2873–2875 (2009).
50. M. Liscidini and J. E. Sipe, "Stimulated emission tomography," *Phys. Rev. Lett.* **111**, 193602 (2013).
51. A. Siegman, *Lasers* (University Science Books, 1986).
52. Y.-C. Liu, D.-J. Guo, R. Yang, C.-W. Sun, J.-C. Duan, Y.-X. Gong, Z. Xie, and S.-N. Zhu, "Narrowband photonic quantum entanglement with counterpropagating domain engineering," *Photon. Res.* **9**, 1998–2005 (2021).
53. P. Kuo, "Optical spectra data for backward-wave spontaneous parametric downconversion," Version 1.0.0, National Institute of Standards and Technology (2022). <https://doi.org/10.18434/mds2-2776>.